Electronic Supplementary Material (ESI) for Physical Chemistry Chemical Physics.

In-Situ Monitoring of Mechanochemical MOF Formation by NMR Relaxation Time Correlation

Madeleine *E. Leger,*[ab] *Jiangfeng Guo,*[b] *Bryce MacMillan,*[b] *Hatem M. Titi,*[c] *Tomislav Friščić,*[c,d] *and Bruce Balcom,*[a,b*] *and Barry A. Blight*[a*]

[a] Department of Chemistry, University of New Brunswick, Fredericton, New Brunswick, E3B 5A3, Canada

[b] UNB MRI Centre, Department of Physics, University of New Brunswick, Fredericton, New Brunswick, E3B 5A3, Canada

[c] Department of Chemistry, McGill University, Montreal, Quebec, H3A 0G4, Canada

[d] School of Chemistry, University of Birmingham University, Birmingham, B15 2TT, UK

* Corresponding author: bjb@unb.ca, b.blight@unb.ca

Supplementary Material

Table of Contents

S1: Methods

Probe and Teflon vials

Figure S1. Doty DS1-874 ^{1}H RF probe, small 7.5 mL Teflon jar, and two small 7 mm zirconia balls.

PXRD

The identities of all reactants were confirmed through X-ray powder patterns and were collected on a Bruker D8 Advance spectrometer in the UNB geochemical and spectrographic facilities. Fine powder samples (gently crushed in mortar when necessary) were packed into the circular well on the sample-holder, after which it was placed on the sample stage and scanned. The diffractometer was equipped with a two-circle (theta-theta) goniometer housed in a radiation safety enclosure. The X-ray source was a sealed, 2.2 kW Cu X-ray tube, maintained at an operating current of 40 kV and 25 mA. The X-ray optics was that of standard Bragg-Brentano para-focusing mode with the X-rays diverging from a divergence slit (1.00 mm) at the tube to strike the sample and then converging through an anti-scatter receiving slit (1.00 mm) and a detector slit (0.20 mm). The goniometer was computer controlled with independent stepper motors and optical encoders for the θ and 2θ circles with the smallest angular step size of 0.0001° 2θ. Samples were scanned in the range of 5-70° 2θ A step size of 0.02° and a step time of 1.0 sec were used during the measurements. A peltier-cooled solid-state [Si(Li)] detector (Sol-X) with a useful energy range of 1 to 60 KeV was used as the detector. No correction was made for K_β radiation. A set of 2° Soller slits were used in order to lower horizontal beam divergence.

The identities of the after-milling products were obtained on a Bruker D2 PHASER diffractometer equipped with a LynxEye linear position sensitive detector (Bruker AXS, Madison, WI, USA), using Ni-filtered CuKα radiation. The data were collected between 2θ 4-50°, at increment of 0.02° and exposure time of 0.3 s.

SEM/EDS

SEM images and EDS data were collected on a JEOL JSM-6400 Scanning Electron Microscope equipped with an EDAX Genesis 4000 Energy Dispersive X-ray (EDS) analyser at the UNB Microscopy and Microanalysis Facility. EDS analysis was performed at an

accelerating voltage of 15 kV and a beam current of 1.5 nA, with a working distance of 14 mm. Collection time was 50 seconds per analysis point.

TGA

TGA data were obtained on a TGA 5500 Discovery by TA Instruments. The samples were heated to 700°C at a rate of 10 °C/min and a gas flow of 25 mL/min.

MR measurement

Solid materials have particularly interesting T_1 -T_2* behaviors. Solids commonly feature very long T_1 values and extremely short T_2 values. This is explained by Bloembergen-Purcell-Pound (BPP) theory which illustrates the theoretical relationship between T_1 and T_2 relaxation times and molecular mobility.[1] BPP theory emphasizes the importance of correlation time and motion in determining MR lifetime. Solids have increasingly large T1 values as molecular and proton mobility decreases, and very short T_2 values. Since T_2* decay is governed by T_2, the T_2* decay of solids is very short. Indeed, in our study, a T_1 of 47.7 s and a T_2* as short as 5.7 μs were measured.

These unusual relaxation times heavily influenced our relaxation measurement and pulse sequence choices. Common relaxation time methodologies to obtain T_1-T_2 data based on multiple spin echoes are not appropriate for solid samples since the short-lived signal decays too rapidly compared to the echo time and long 90° and 180° pulses. A typical pulse sequence to obtain bulk T_1-T_2* data employs inversion recovery, with FIDs acquired as a function of recovery time. This sequence is problematic since the minimum observation time of the sequence is too long to observe the short-lived T_2* signal.

To keep the measurements in this study straightforward, we utilized a saturation recovery pulse sequence to obtain T_1-T_2* data at room temperature. Saturation recovery (figure 4b) is the most appropriate MR sequence for solid-state analysis for a few reasons. First, it is a quick measurement. There is no need to wait five times the value of T_1 or to use a full 90° pulse during the sequence, which greatly reduces the minimum observation time of the sequence. Also, saturation recovery allows the measurement of very short T_2* decays because of the lack of multiple spin echoes or long RF pulses. To assure the acquisition of the short-lived FID decay, a short duration RF pulse, 5 μs, was utilized in this study. It is also important to have short acquisition deadtimes to have a chance at measuring the very short T_2* component. The deadtime (dt) was 4 μs.

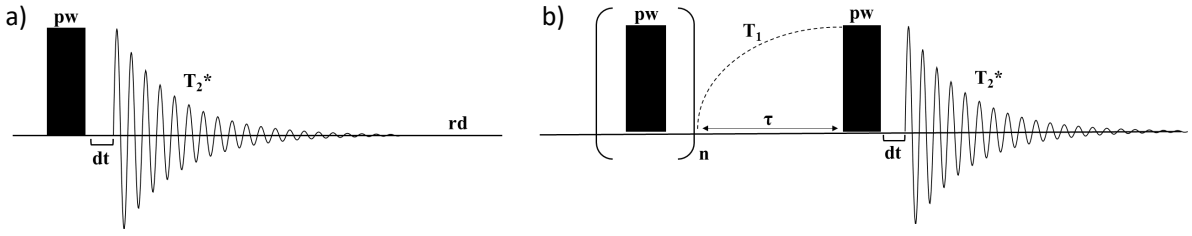

Figure S2. The pulse sequence of a (a) FID and (b) saturation recovery with some important parameters shown. The pulse width (pw) and probe dead time (dt) must be kept short to ensure capturing short-lived signal from the solid samples. In the FID sequence, the recycle delay (rd) is an important factor in measurement time since its value should be equal to five times the value of the longest T_1 in the sample. In the saturation recovery sequence, a series (n) of pw pulses are applied followed by a series of different lengths of recovery times (τ). The T_2* values are obtained from the FID curves, while the T_1 weighing depends on the longitudinal magnetization recovery after saturation.

Section S2: Relaxation Time Values

	Sample	Peak (T_1, T_2*) / (s, μs)	1	2	3
Zn-MOF-74	Zinc oxide		(0.14, 9.7)	(0.96, 12.1)	
	2,5-dihydroxyterephthalic acid		(0.11, 12.1)	(47.7, 12.1)	
	Before milling		(0.63, 416)		
	Milling 30 minutes		(0.10, 432)	(7.29, 4.09)	
	After milling		(0.012, 106)	(0.20, 6.8)	(11.2, 7.6)
ZIF-8	Zinc oxide		(0.14, 9.7)	(0.96, 12.1)	
	2-methylimidazole		(0.17, 9.1)	(24.9, 9.1)	
	Before milling		(2.30, 432)	(0.15, 10.5)	(30.9, 10.5)
	After milling		(0.78, 210)	(0.83, 10.5)	(28.8, 10.5)
	After milling rinsed		(1.04, 598)	(0.08, 10.1)	(1.04, 10.5)

Table S1. Relaxation times of ZIF-8 and MOF-74 synthesis. (corresponding numbered plots below)

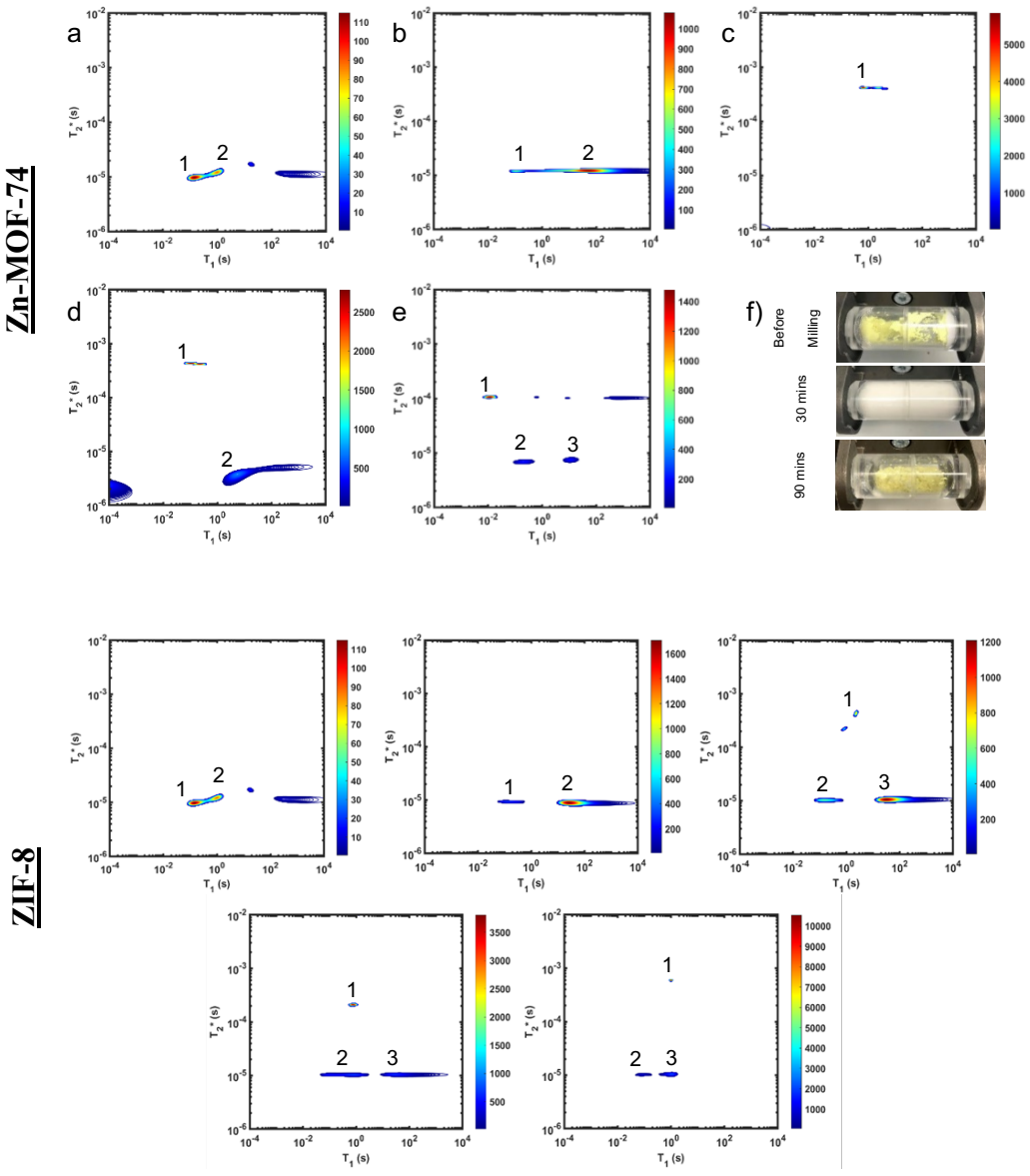

	Sample	Peak (T_1, T_2*) / (s, µs)	1	2	3
Exp.	Reactants pre-milling		(2.30, 432)	(0.15, 10.5)	(30.9, 10.5)
	ZIF-8 as synthesized		(0.78, 210)	(0.83, 10.5)	(28.8, 10.5)
Non-Exp.	Reactants pre-milling		(2.30, 387)	(0.16, 18.6)	(33.2, 20.8)
	ZIF-8 as synthesized		(0.78, 210)	(0.90, 20.0)	(24.9, 21.5)

Table S2. Relaxation times of ZIF-8 synthesis comparing exponential and non-exponential processing. (corresponding numbered plots below)

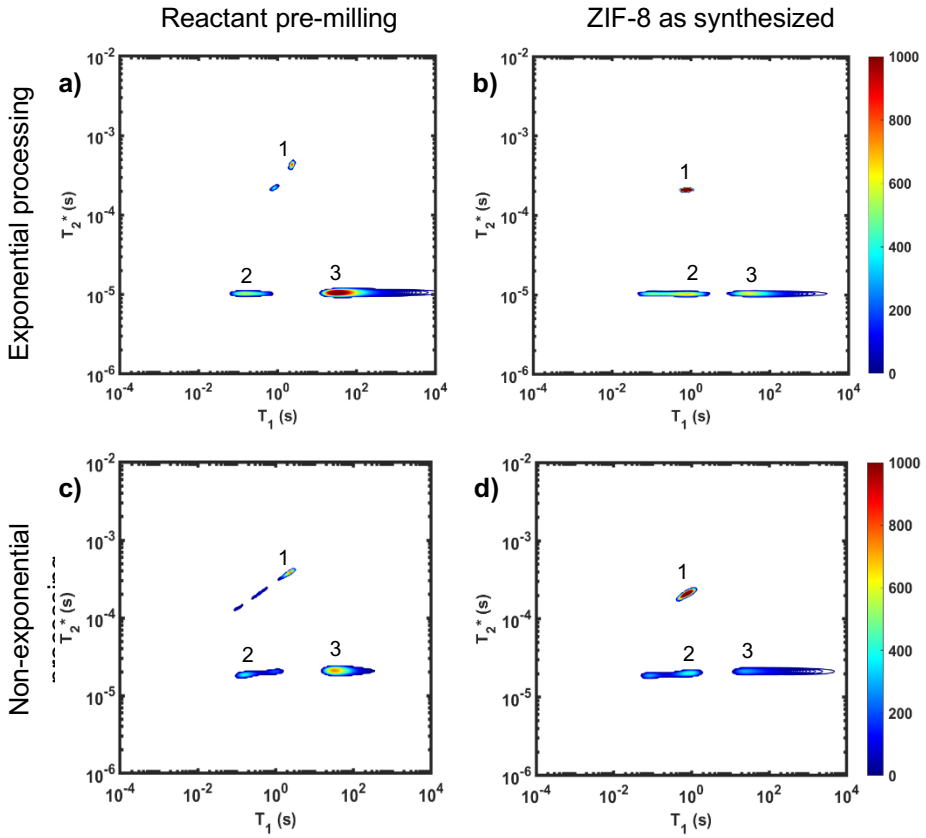

S3: 1D Relaxation Time Plots

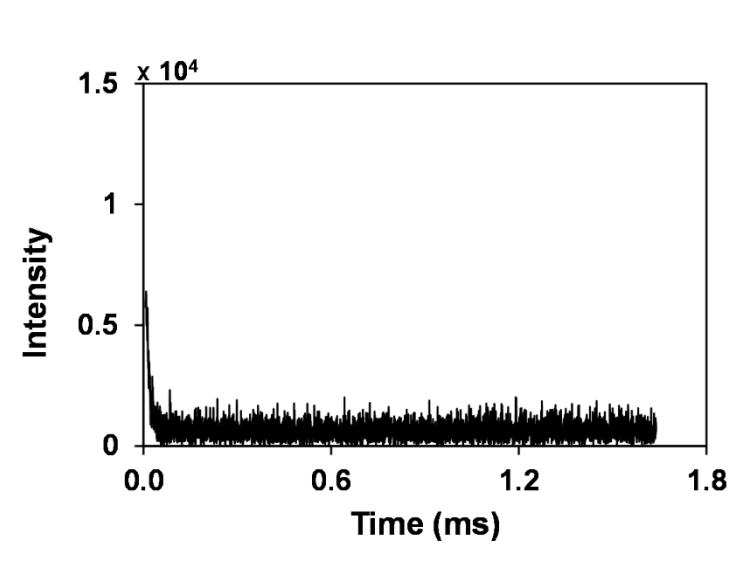

Figure S3. Free induction decay (FID) measurement of T_2* in zinc oxide sample.

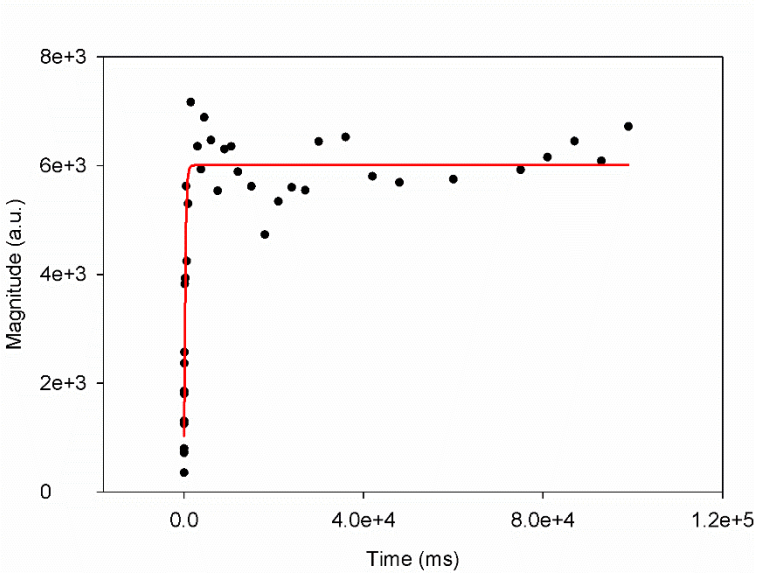

Figure S4. Saturation recovery measurement of T_1 in zinc oxide sample.

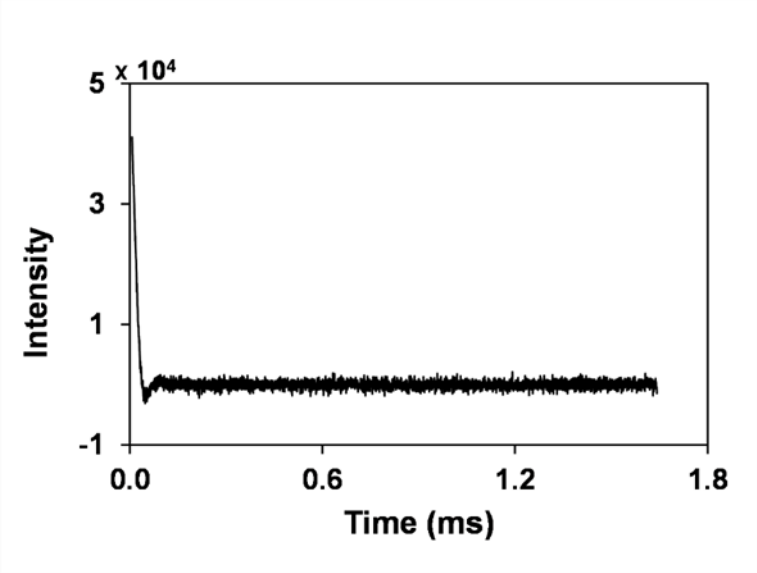

Figure S5. Free induction decay (FID) measurement of T_2* in 2,5-dihydroxyterephthalic acid sample.

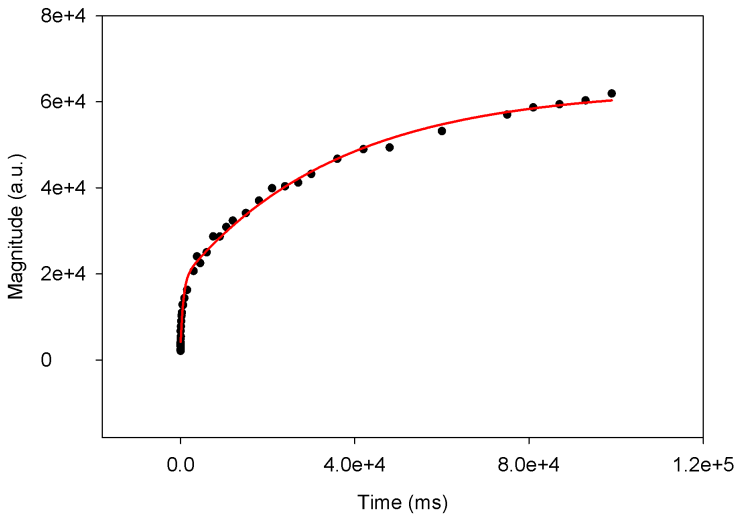

Figure S6. Saturation recovery measurement of T_1 in 2,5-dihydroxyterephthalic acid sample.

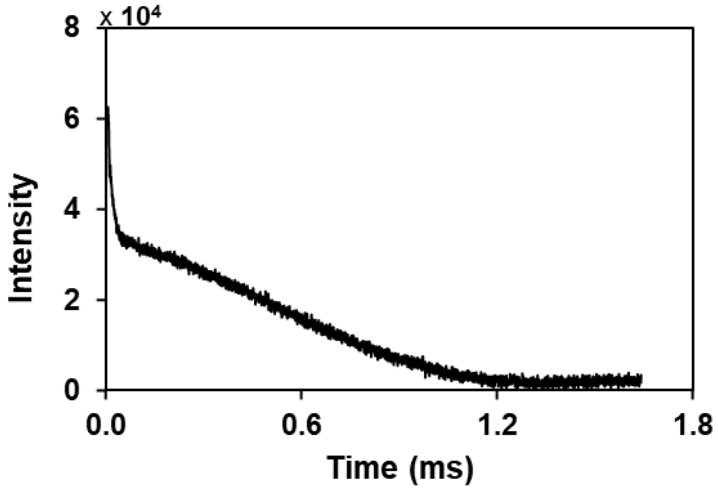

Figure S7. Free induction decay (FID) measurement of T_2* in Zn-MOF-74 mixture before milling sample.

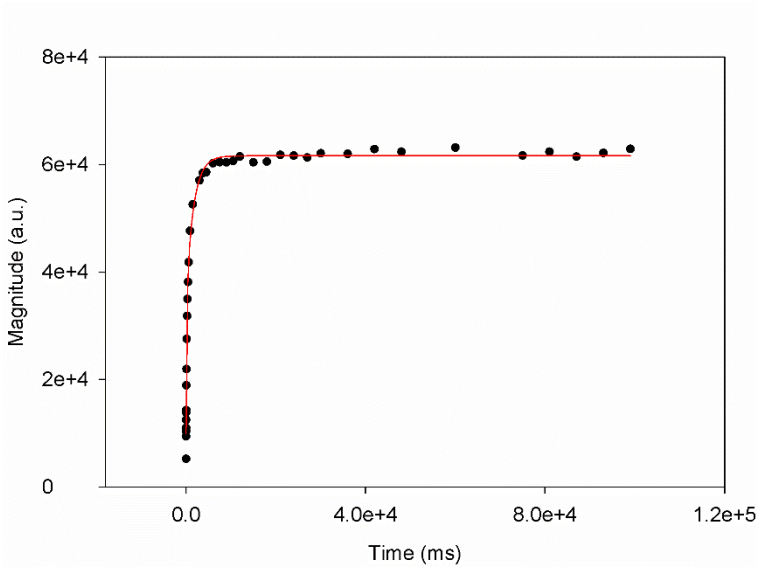

Figure S8. Saturation recovery measurement of T_1 in Zn-MOF-74 mixture before milling sample.

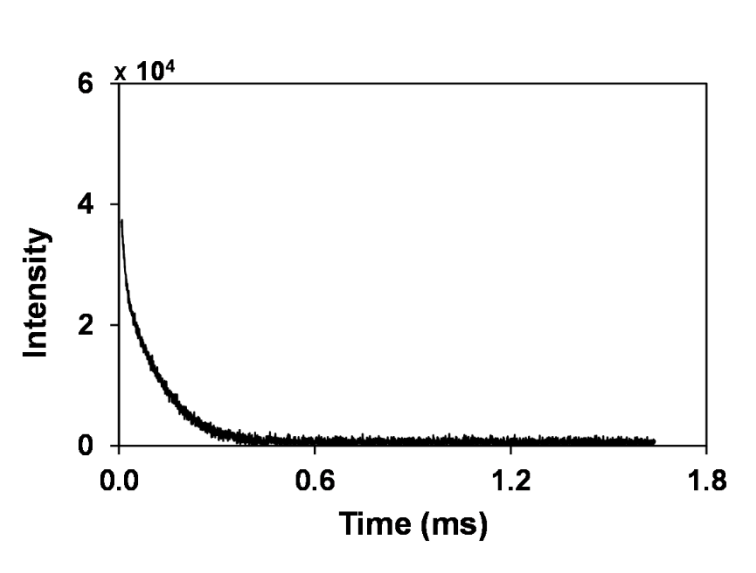

Figure S9. Free induction decay (FID) measurement of T_2* in Zn-MOF-74 as synthesized sample.

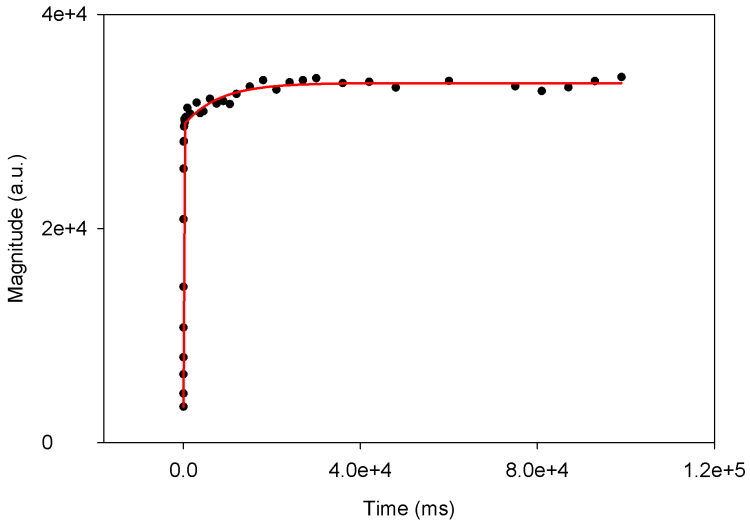

Figure S10. Saturation recovery measurement of T_1 in Zn-MOF-74 as synthesized sample.

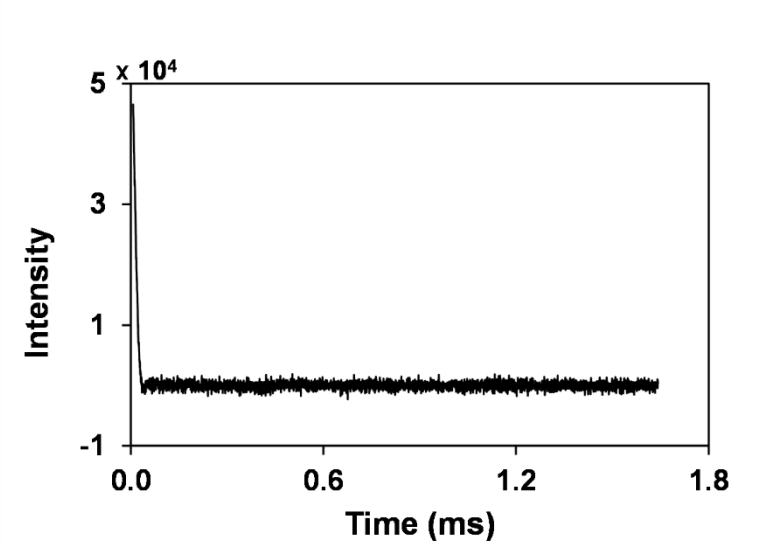

Figure S11. Free induction decay (FID) measurement of T_2* in 2-methylimidazole sample.

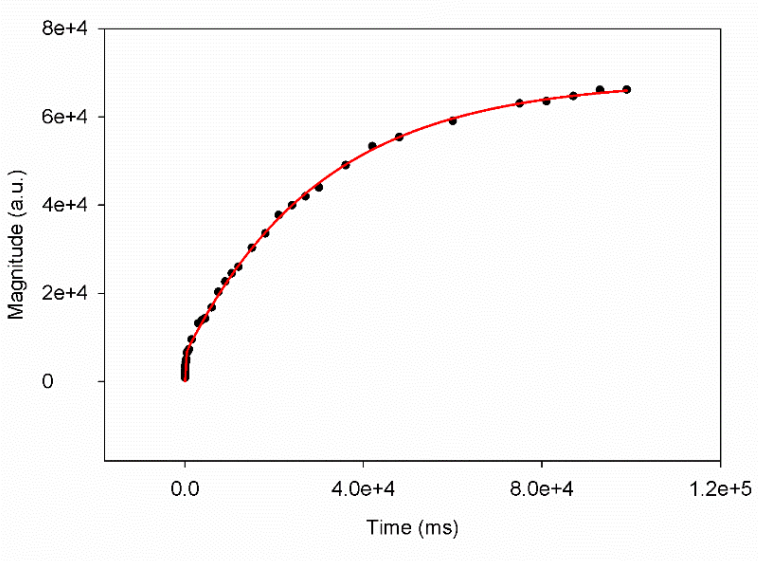

Figure S12. Saturation recovery measurement of T_1 in 2-methylimidazole sample.

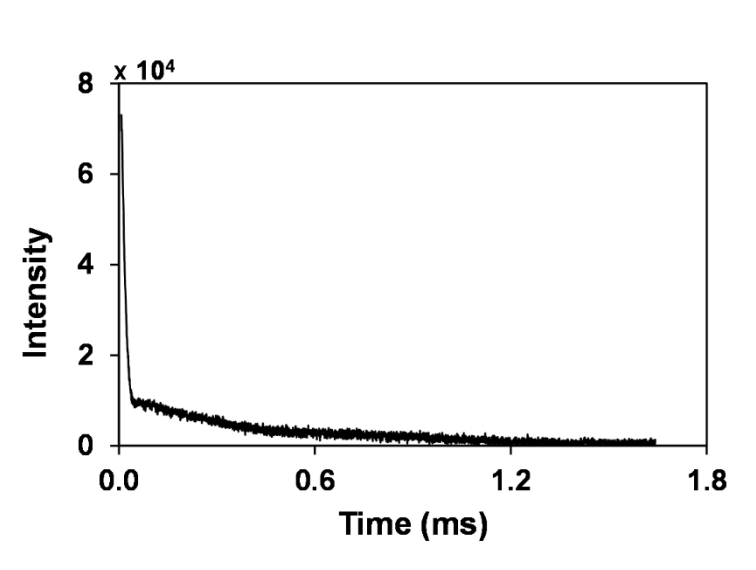

Figure S13. Free induction decay (FID) measurement of T_2* in ZIF-8 mixture before milling sample.

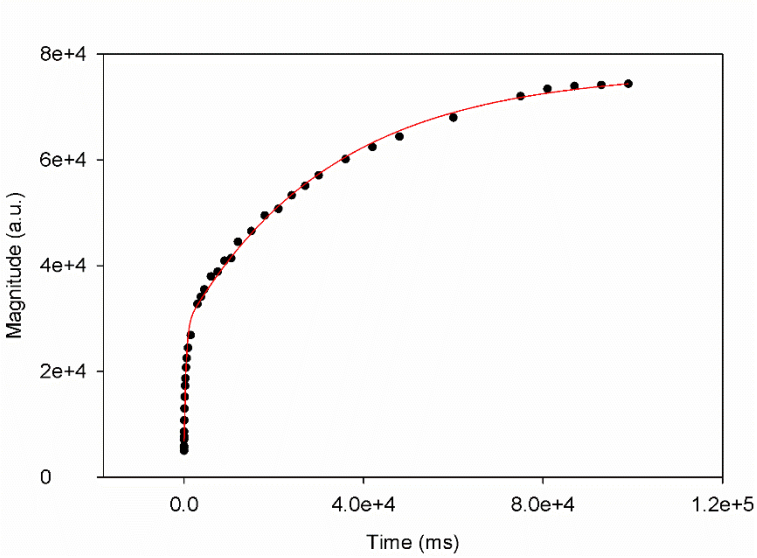

Figure S14. Saturation recovery measurement of T_1 in ZIF-8 mixture before milling sample.

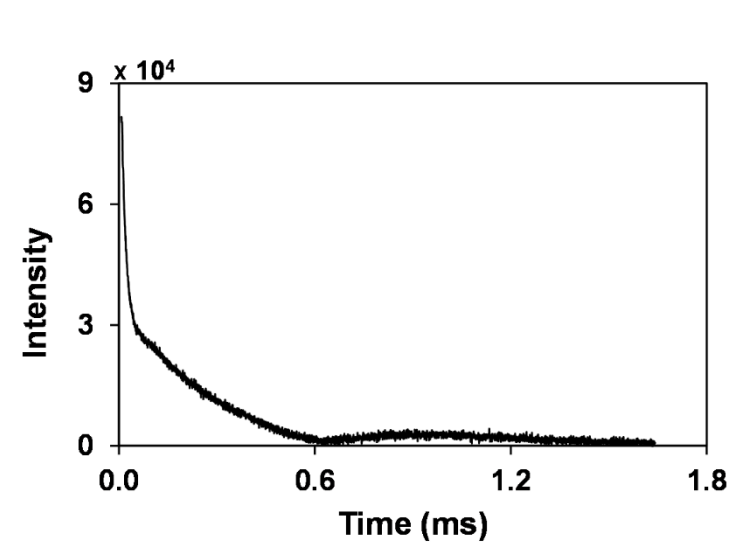

Figure S15. Free induction decay (FID) measurement of T_2* in ZIF-8 as synthesized sample.

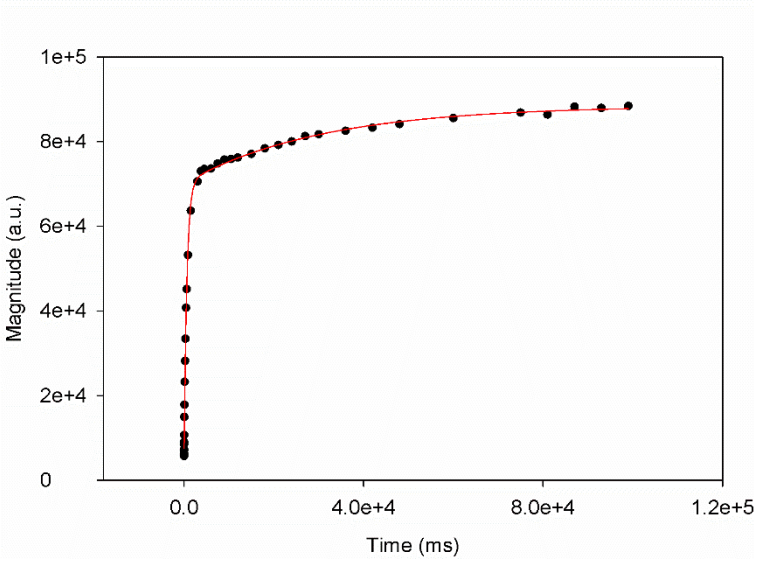

Figure S16. Saturation recovery measurement of T_1 in ZIF-8 as synthesized sample.

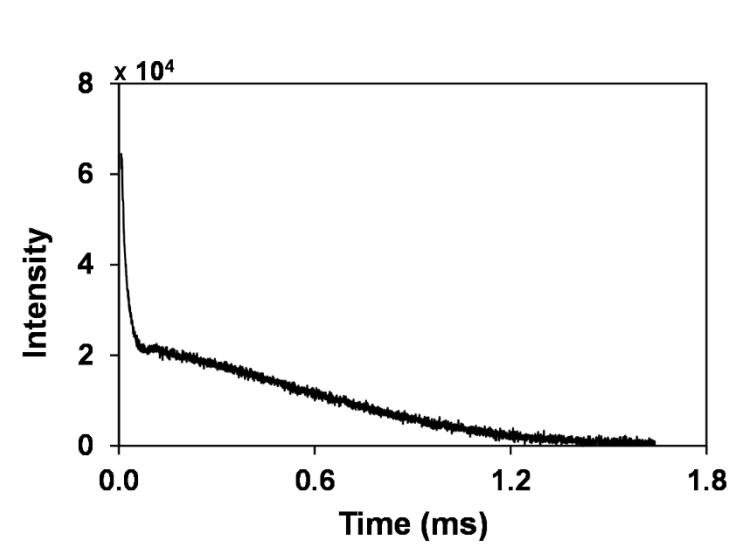

Figure S17. Free induction decay (FID) measurement of T_2* in ZIF-8 rinsed and dried sample.

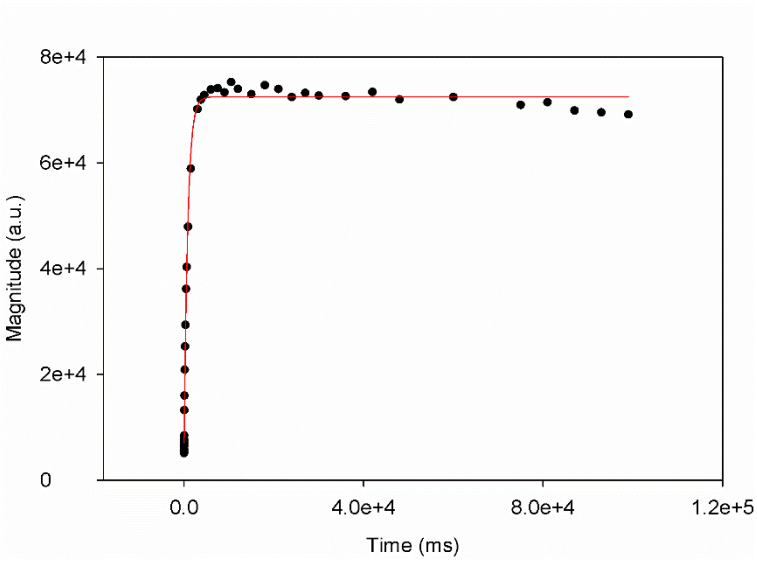

Figure S18. Saturation recovery measurement of T_1 in ZIF-8 rinsed and dried sample.

S4: Non-Exponential Relaxation Time Correlation Plots

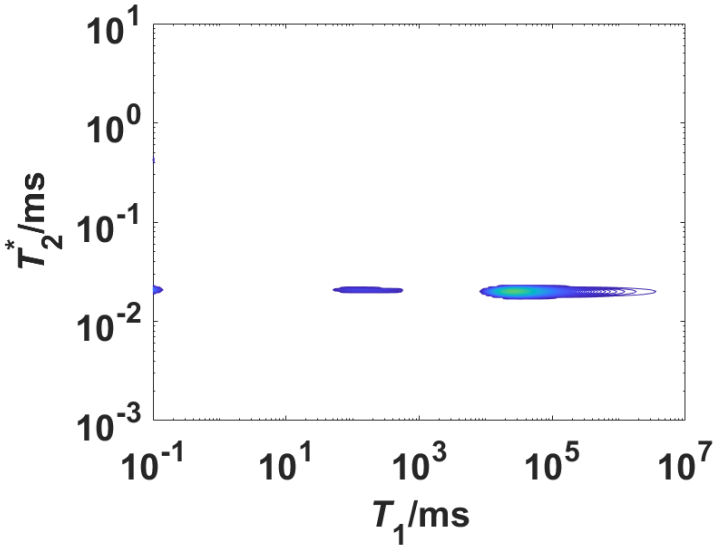

Figure S19. T_1-T_2* correlation plot of 2-methylimidazole, using non-exponential processing.

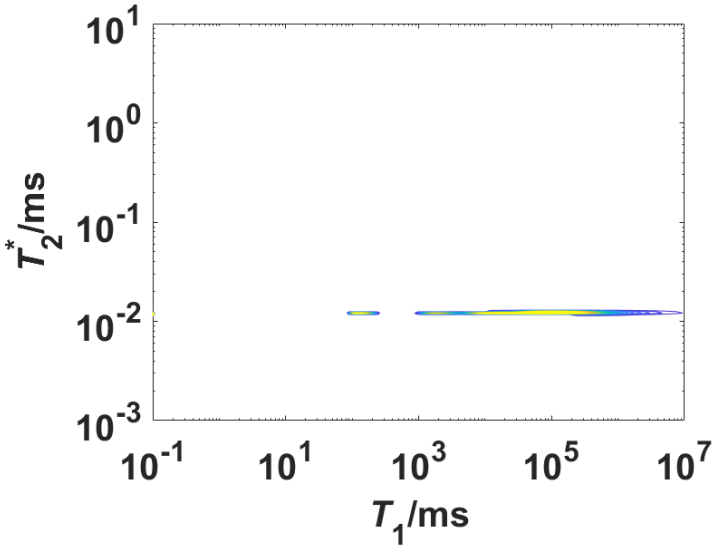

Figure S20. T_1-T_2* correlation plot of 2,5-dihydroxyterephthalic acid, using non-exponential processing.

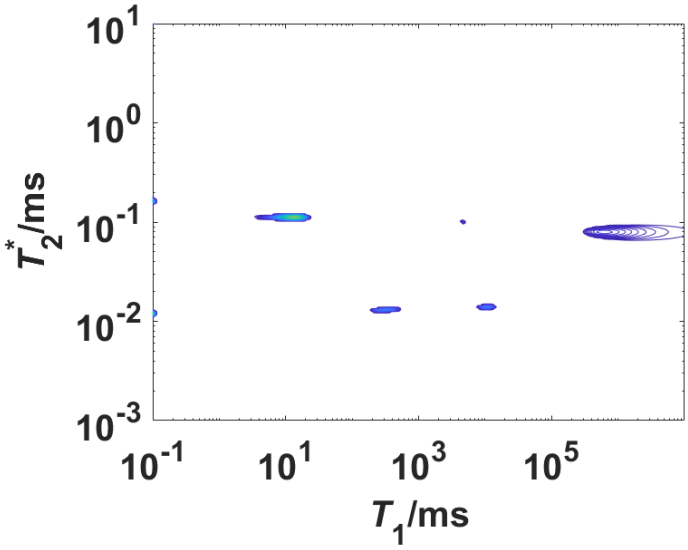

Figure S21. T_1-T_2* correlation plot of Zn-MOF-74 after milling, using non-exponential processing.

S5: PXRD Analysis

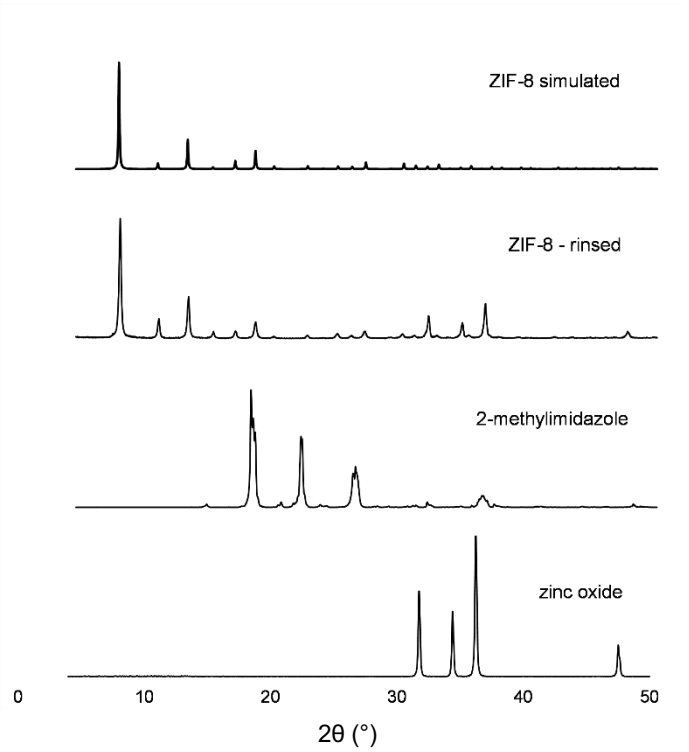

Figure S22. PXRD data of the ZIF-8 reaction. Simulated data obtained using Mercury.[2]

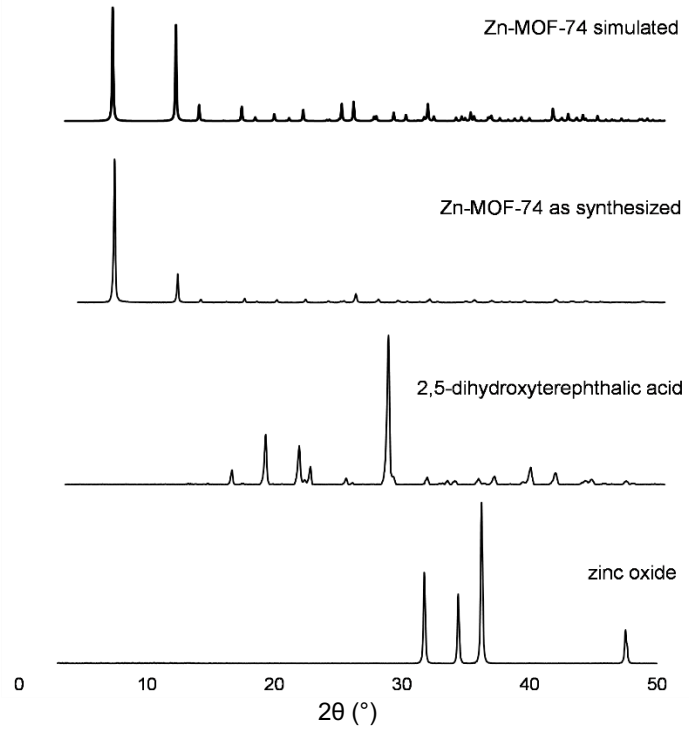

Figure S23. PXRD data of the Zn-MOF-74 reaction. Simulated data obtained using Mercury.[2]

S6: SEM and EDS Analysis

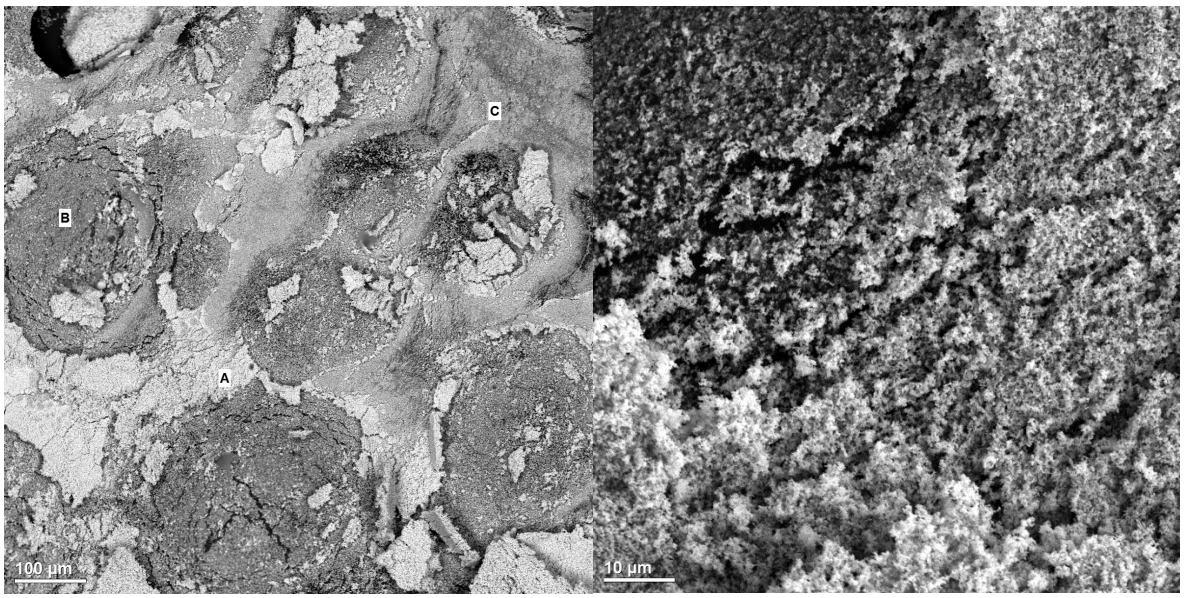

(a) (b)

Figure S24. SEM micrographs of zinc oxide at 100 µm (a) and 10 µm (b).

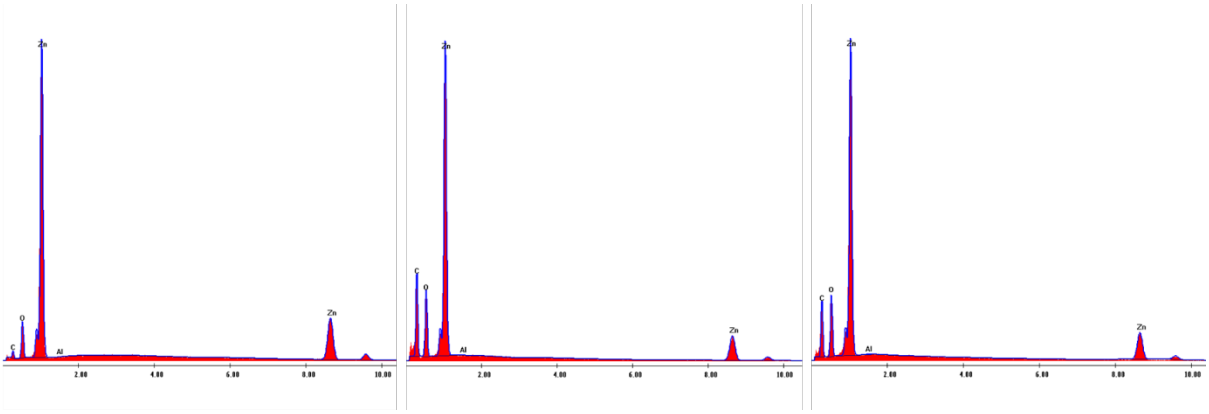

(a) (b) (c)

Figure S25. EDS analysis of zinc oxide (figure S24a, 100 µm).

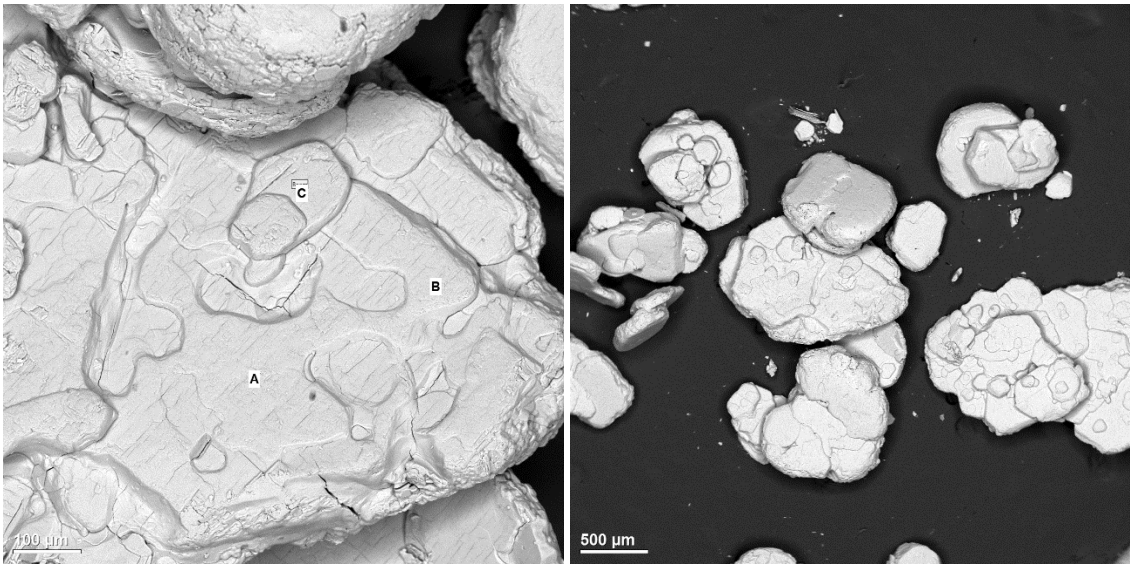

(a) (b)

Figure S26. SEM micrographs of zinc acetate dihydrate at 100 µm (a) and 500 µm (b).

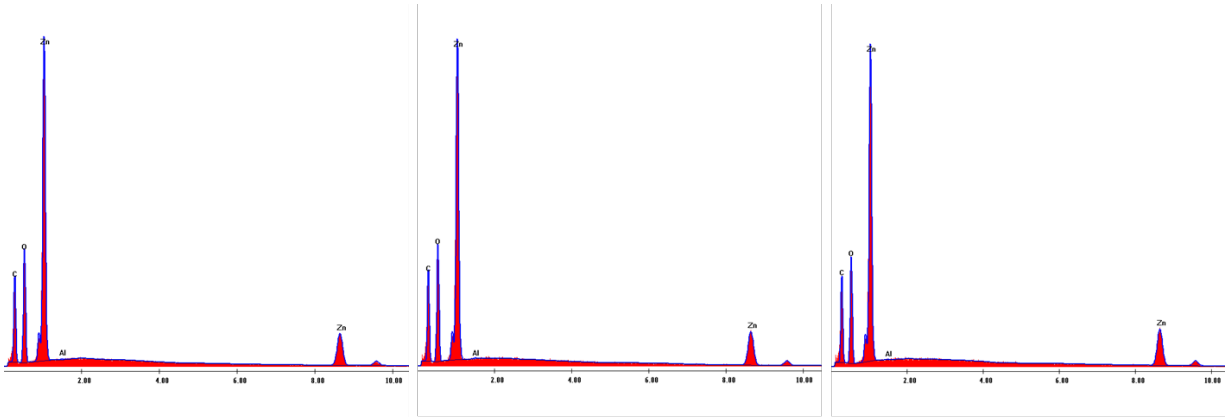

(a) (b) (c)

Figure S27. EDS analysis of zinc acetate dihydrate (figure S26a, 100 µm).

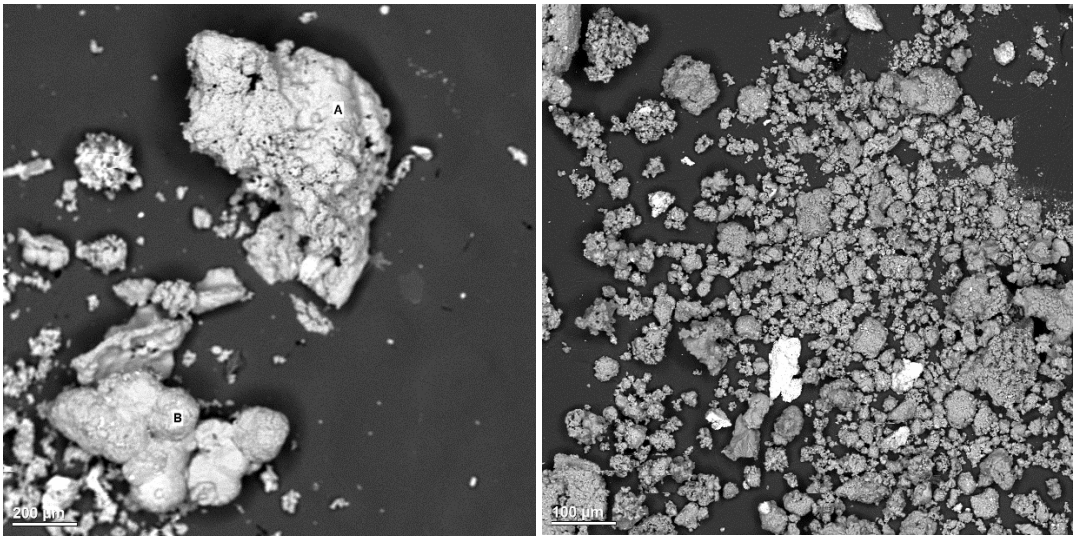

Figure S28. SEM micrographs of ZIF-8 after milling at 200 µm (a) and 100 µm (b).

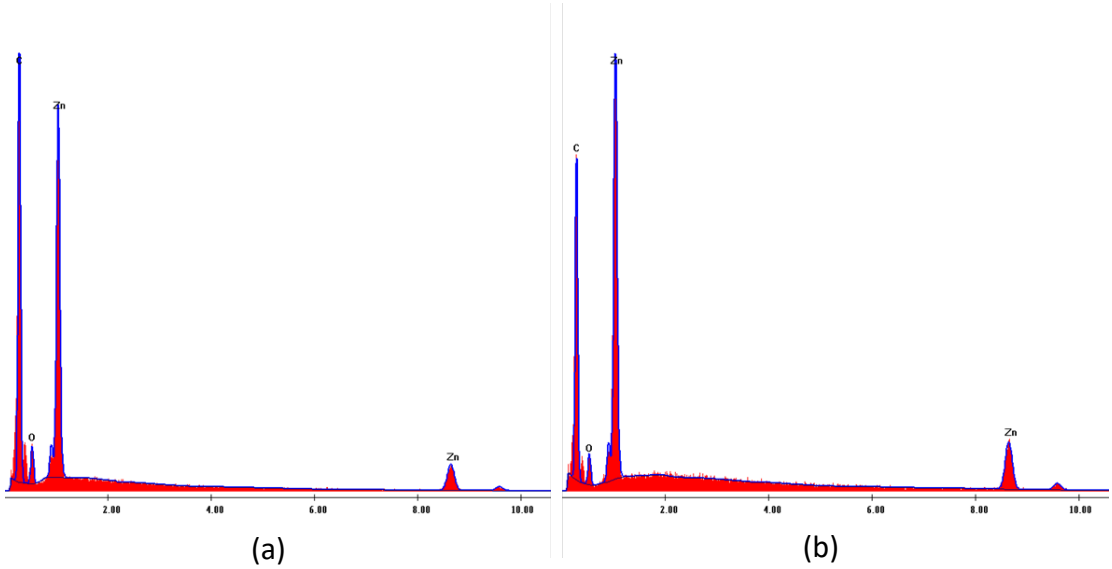

Figure S29. EDS analysis of ZIF-8 (figure S28a, 200 µm).

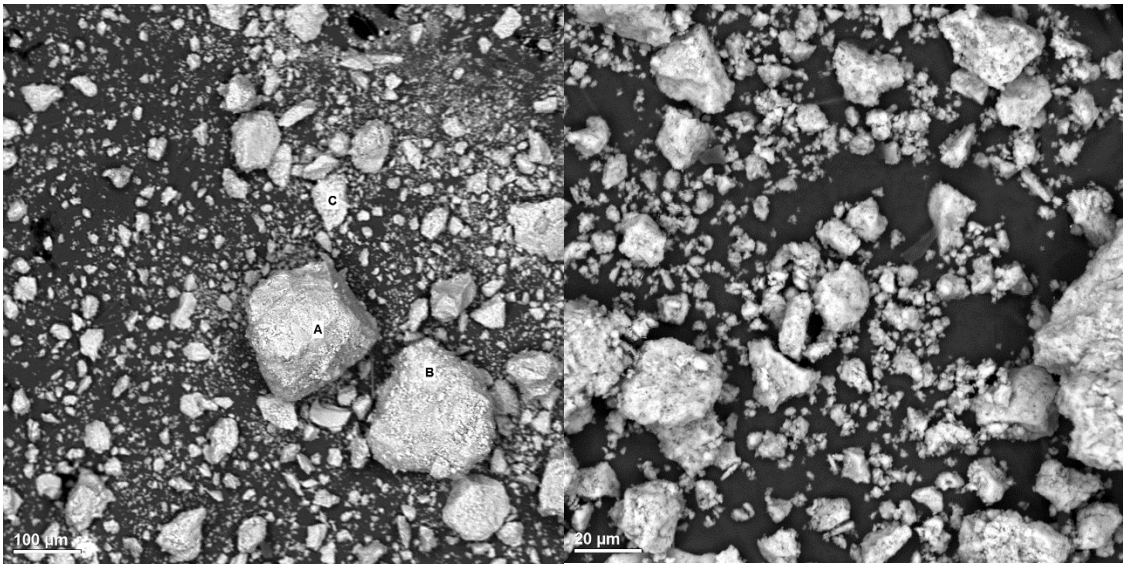

(a) (b)

Figure S30. SEM micrographs of Zn-MOF-74 after milling at 100 µm (a) and 20 µm (b).

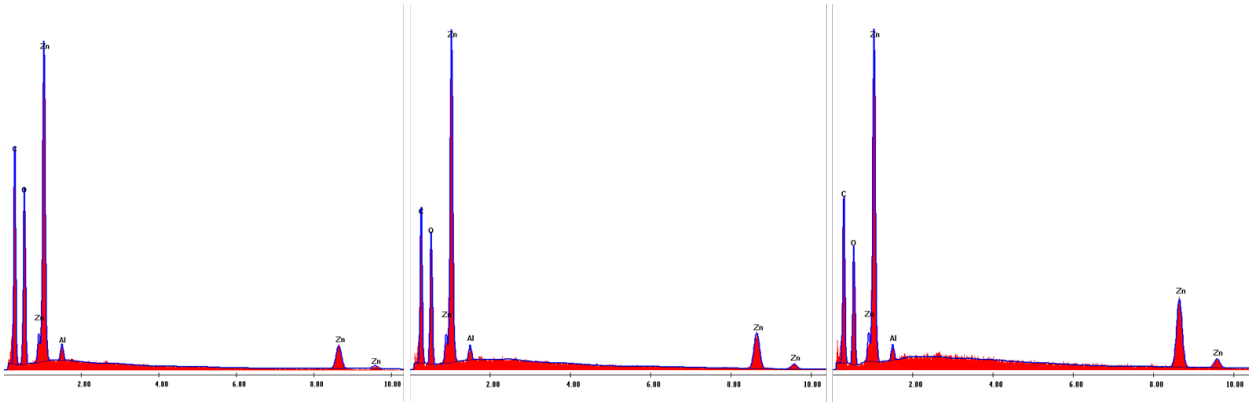

(a) (b) (c)

Figure S31. EDS analysis of Zn-MOF-74 (figure S30a, 100 µm).

S7: TGA Analysis

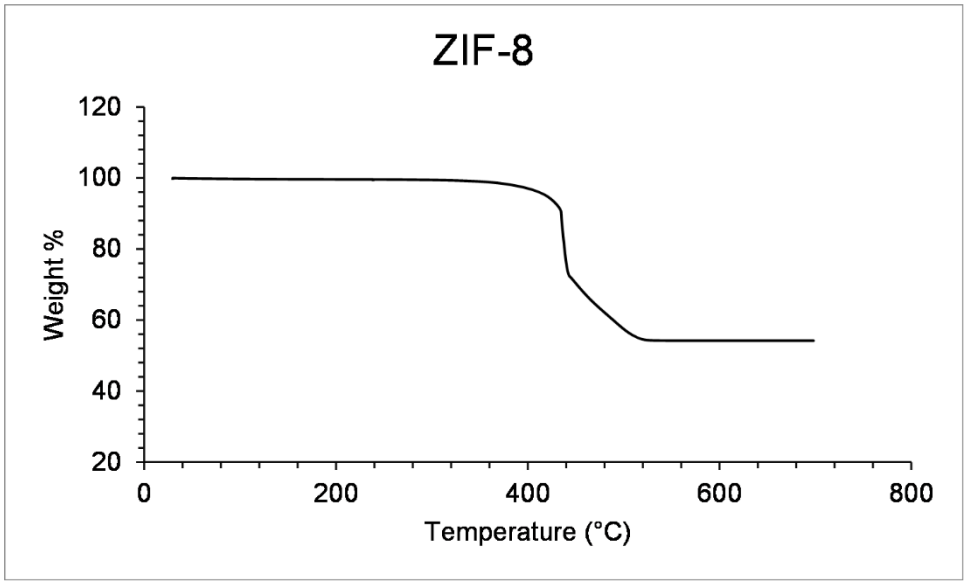

Figure S32. TGA analysis of ZIF-8.

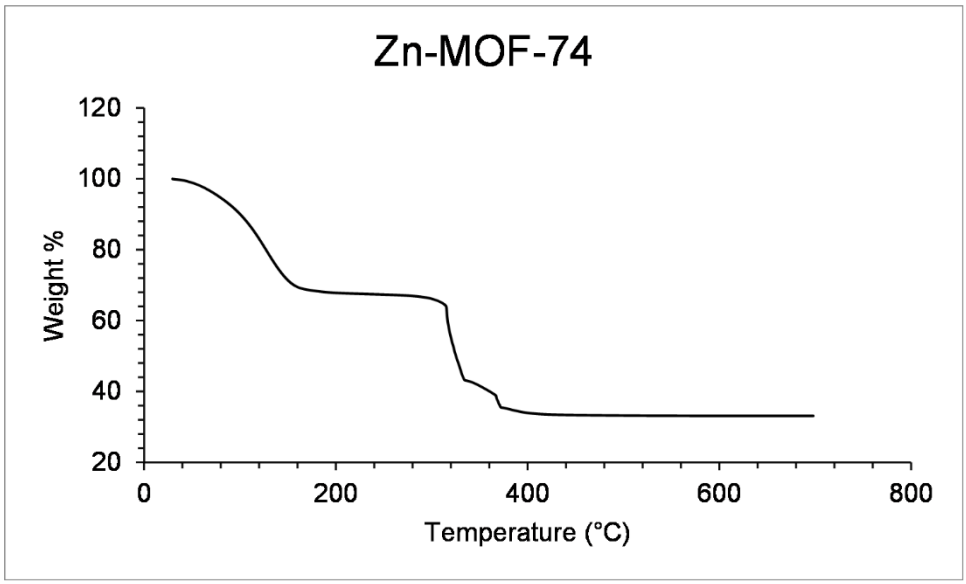

Figure S33. TGA analysis of Zn-MOF-74.

S8: References

(1) Bloembergen, N.; Purcell, E. M.; Pound, R. v. Relaxation Effects in Nuclear Magnetic Resonance Absorption. *Phys. Rev.* **1948**, *73* (7), 679–712. https://doi.org/10.1103/PhysRev.73.679.

(2) Macrae, C. F.; Sovago, I.; Cottrell, S. J.; Galek, P. T. A.; McCabe, P.; Pidcock, E.; Platings, M.; Shields, G. P.; Stevens, J. S.; Towler, M.; Wood, P. A.; IUCr. Mercury 4.0: From Visualization to Analysis, Design and Prediction. *J. Appl. Cryst.* **2020**, *53*, 226–235. https://doi.org/10.1107/S1600576719014092.